Reactivity and Mechanism Studies of Hydrogen Evolution Catalyzed by Copper Corroles

Haitao Lei,[†,∥] Huayi Fang,[‡,∥] Yongzhen Han,[†] Wenzhen Lai,*[,†] Xuefeng Fu,*[,‡] and Rui Cao*[,†,§]

[†]Department of Chemistry, Renmin University of China, Beijing 100872, China
[‡]College of Chemistry and Molecular Engineering, Peking University, Beijing 100871, China
[§]Department of Chemistry and Chemical Engineering, Beijing University of Technology, Beijing 100124, China

ⓢ *Supporting Information*

ABSTRACT: Several copper corrole complexes were synthesized, and their catalytic activities for hydrogen (H_2) evolution were examined. Our results showed that substituents at the *meso* positions of corrole macrocycles played significant roles in regulating the redox and thus the catalytic properties of copper corrole complexes: strong electron-withdrawing substituents can improve the catalysis for hydrogen evolution, while electron-donating substituents are not favored in this system. The copper complex of 5,15-pentafluorophenyl-10-(4-nitrophenyl)corrole (**1**) was shown to have the best electrocatalytic performance among copper corroles examined. Complex **1** can electrocatalyze H_2 evolution using trifluoro-acetic acid (TFA) as the proton source in acetonitrile. In cyclic voltammetry, the value of $i_{cat}/i_p = 303$ (i_{cat} is the catalytic current, i_p is the one-electron peak current of **1** in the absence of acid) at a scan rate of 100 mV s^{-1} and 20 °C is remarkable. Electrochemical and spectroscopic measurements revealed that **1** has the desired stability in concentrated TFA acid solution and is unchanged by functioning as an electrocatalyst. Stopped-flow, spectroelectrochemistry, and theoretical studies provided valuable insights into the mechanism of hydrogen evolution mediated by **1**. Doubly reduced **1** is the catalytic active species that reacts with a proton to give the hydride intermediate for subsequent generation of H_2.

KEYWORDS: hydrogen evolution, copper corroles, electrocatalysis, reduction, stopped-flow
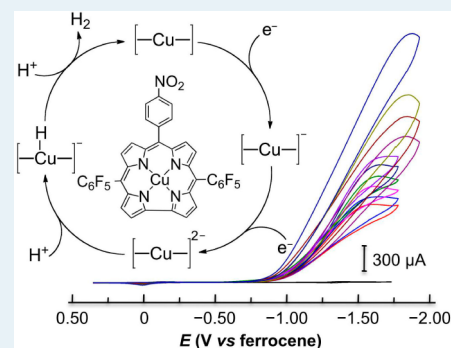
■ INTRODUCTION

Globally increasing energy demand and environmental concerns related to the use of fossil fuels have made energy research the paramount task for our society.[1−7] H_2 has emerged as an ideal energy source because it is carbon-free, renewable, and produces only water as a combustion product.[8−16] Electrochemical reduction of protons is an effective and convenient process to convert electrical energy to chemical energy through generating H_2.[17−19] This process is rapidly gaining attention as a vital paradigm for future energy conversion, storage, and delivery.[20,21] In nature, hydrogenases catalyze the reversible reduction of protons with low overpotentials and high turnover frequencies up to 9000 s^{-1}.[22,23] However, the challenge in obtaining and using these enzymes in non-natural environments obstructs their practical applications,[24] even though the use of hydrogenases with chemical modifications under ambient environments is known in the literature.[25,26] Platinum is very active in electrocatalytic H_2 production,[8] but utilization of this noble metal is limited by its low natural abundance and high cost. Less-expensive earth-abundant transition metal complexes have therefore attracted major attention to serve as catalysts for hydrogen evolution reaction (HER).[27−31] Recent focus on the development of HER catalysts has resulted in identifying complexes of several

earth-abundant metals including iron,[32−35] cobalt,[36−45] nickel,[12,20,46] and molybdenum[47−49] active for this catalysis, but the catalyst design features still fall short in either catalytic efficiency[20,48] or stability in required concentrated acid environments.[20] Therefore, the discovery of new metal systems that can offer highly efficient and robust HER catalysts remains a substantial challenge in the energy research community.

Copper plays significant roles in numerous redox processes in biological systems.[50] Synthetic copper complexes have also been extensively investigated because of their prominent biomimetic and redox chemistry.[50,51] Although Cu-based materials have been used as catalysts or cocatalysts for the reduction of protons and carbon dioxide,[52−59] copper-containing complexes that can catalyze H_2 production have rarely been recognized. One possible reason is that the reduction potential of low-valent copper species is typically too positive to reduce protons. Recently, Sun and Wang reported the first example of a homogeneous copper electrocatalyst for water reduction.[60] The polypyridine ligand used in this work was considered to be able to stabilize two-electron
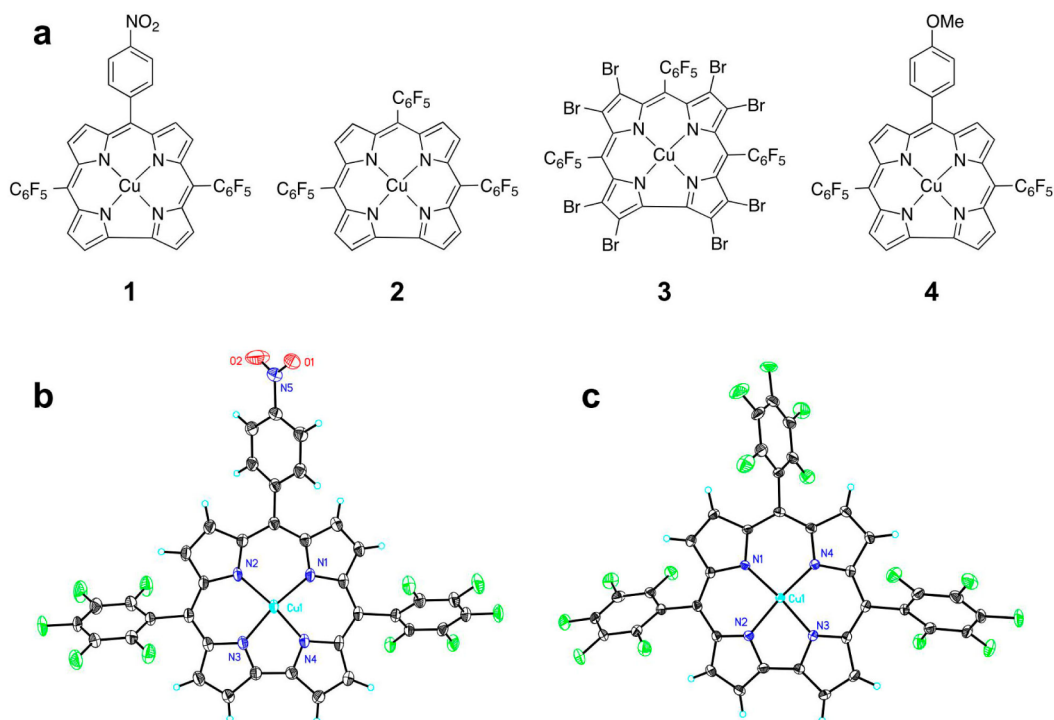
Figure 1. Chemical structures of copper corroles. (a) Molecular structures of complexes **1**−**4**. (b) Thermal ellipsoid plot (50% probability) of the X-ray structure of **1**. (c) Thermal ellipsoid plot (50% probability) of the X-ray structure of **2**. The average Cu−N bond distances are 1.893(4) and 1.889(4) Å for **1** and **2**, respectively.
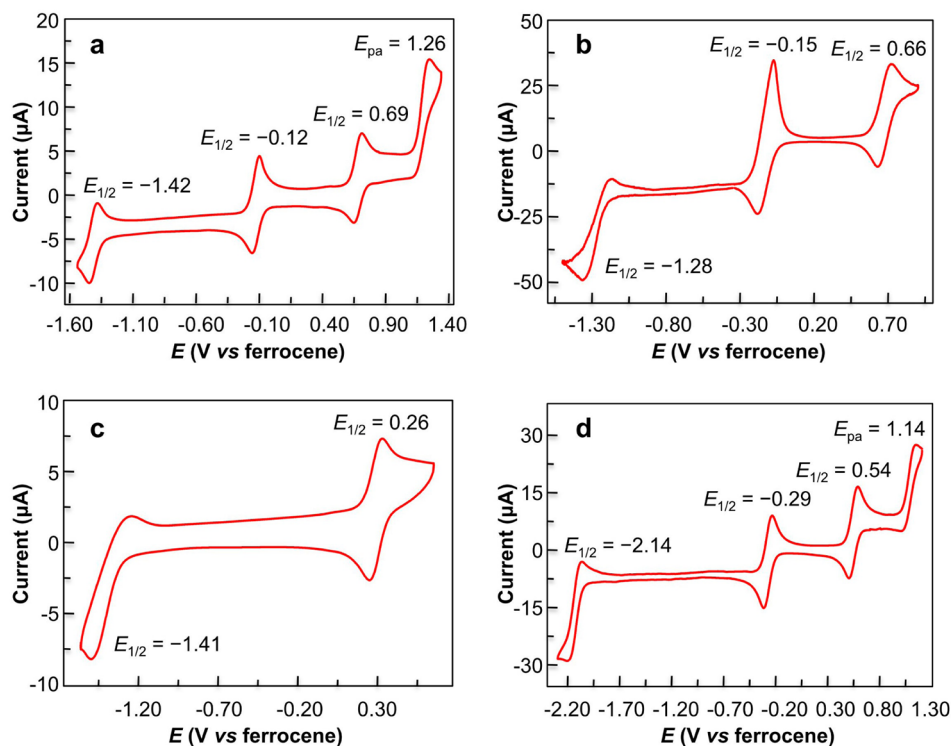

Figure 2. Cyclic voltammograms of complexes **1**−**4**. (a) A 0.30 mM acetonitrile solution of **1**. (b) A 1.0 mM acetonitrile solution of **2**. (c) A 0.13 mM acetonitrile solution of **3**. (d) A 0.75 mM acetonitrile solution of **4**. Measurements were performed using 0.1 M $(Bu_4N)PF_6$ as the electrolyte with a scan rate of 100 mV s^{-1}.

reduced copper center that subsequently reduces protons. Recent works from Dey and Gross[61,62] and also from us[63] showed that cobalt corroles were efficient in catalyzing HER and the redox noninnocent corrole macrocycles played a significant role in these processes by tuning the redox properties of incorporated metal centers. Herein we report on copper corroles as another example of copper-based molecular HER catalysts. The remarkable activity (i_{cat}/i_p =

303 at a scan rate of 100 mV s^{-1} and 20 °C) and stability of copper corroles in concentrated TFA acid solutions are noteworthy. The combination of stopped-flow and spectroelectrochemistry techniques and also theoretical studies suggested that two-electron reduced **1** is the catalytic active species that reduces a proton to form a copper hydride intermediate for subsequent H$_2$ evolution.

RESULTS AND DISCUSSION

Synthesis and Electrochemistry. Copper corroles **1–4** (Figure 1) were synthesized by metalation of corresponding corroles with copper(II) acetate. Purification by column chromatography and recrystallization afforded crystalline samples of **1–4** in moderate yields. X-ray structures of **1** and **2** showed that the Cu center was coordinated to the corrole ligand to give a distorted square planar geometry with a saddling structural character.[64,65] In complexes **1–4**, a formally d^8 Cu(III) center was suggested based on the short Cu–N bond distances (Figure 1) and the diamagnetism observed in nuclear magnetic resonance (NMR) spectroscopy (Figure S5 and S6). A significant feature of neutral copper corroles ([(Cor)Cu]^0) is that the [(Cor^{3-})Cu^{3+}] formulation with a Cu(III) center and the regular corrole trianion and the formulation as a Cu(II) center with a corrolato dianion radical [(Cor$^{•2-}$)Cu^{2+}] are almost degenerate in energy.[66] As the exact electronic structure of copper corroles is not our interest, for simplicity, the neutral [(Cor)Cu]^0 formulation will be used hereafter.

The cyclic voltammogram (CV) of **1** in dry acetonitrile showed two reduction waves $E_{1/2}$ = −0.12 V and $E_{1/2}$ = −1.42 V versus ferrocene (all potentials reported herein are referenced to ferrocene) and two oxidation waves $E_{1/2}$ = 0.69 V and E_{pa} = 1.26 V (Figure 2a). The peak separation ΔE_p for the three reversible redox couples was measured to be ∼78 mV, implying three one-electron events (ΔE_p of ferrocene = 75 mV). On the basis of previous knowledge[66,67] and our studies,[63,68−70] the first oxidation of **1** was assigned to corrole-centered giving [(Cor)Cu]$^{•+}$, and the first and second reductions produce [(Cor)Cu]$^-$ and [(Cor)Cu]$^{2-}$, respectively. Significantly, upon addition of TFA (pK_a = 12.7 in acetonitrile),[36] a large electrocatalytic current for proton reduction appeared with the onset of catalytic wave at −0.95 V (Figure 3). This catalytic current peaks at −1.65 V, and has half the maximum current achieved at a potential of −1.35 V.

As the thermodynamic potential required for the reduction of TFA in acetonitrile is known to be −0.90 V,[71] the overpotential for HER with **1** is determined to be ∼450 mV based on its half-wave potential (Figure 3).[20] The catalytic H$_2$ production was supported by concomitant formation of a large amount of gas bubbles on the surface of the glassy carbon working electrode. Importantly, control experiments by adding TFA to an acetonitrile solution of ligand 5,15-pentafluorophenyl-10-(4-nitrophenyl)corrole showed no catalytic current under similar conditions. We also carried out control experiments using free Cu(II) ions, which resulted in the deposition of Cu films on the electrode and displayed very different electrochemical behaviors as compared to **1**. In addition, the catalytic current had a linear dependence on the concentration of **1** (Figure S7), which is a strong evidence for homogeneous catalysis. These results suggest that copper corrole **1** is a molecular catalyst for proton reduction.

In comparison to **1**, although **2** has similar reduction potentials (Figure 2b, $E_{1/2}$ = −0.15 V; $E_{1/2}$ = −1.28 V),
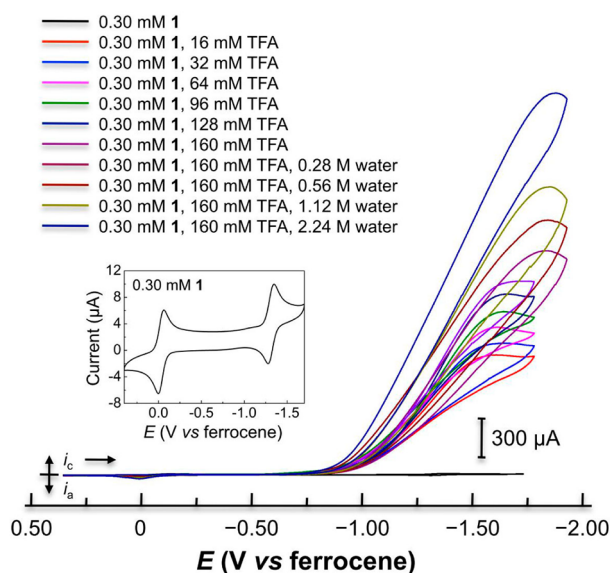

Figure 3. Successive cyclic voltammograms of 0.30 mM **1** in acetonitrile with increasing concentrations of TFA followed by addition of small aliquots of water. Conditions: 0.1 M (Bu$_4$N)PF$_6$ as the electrolyte; 3 mm glassy-carbon working electrode; 100 mV s^{-1} scan rate; 20 °C.

complex **2** degrades rapidly in acidic solution through an oxidative dimerization mechanism, a phenomenon which has been reported by Gross and co-workers.[66] It is suggested that the electronic structure of corrole molecules is likely to affect their stabilities toward this oxidative dimerization. For example, the cobalt corrole analogue of complex **2** also undergoes a spontaneous dimerization in solution, while cobalt complexes of the same corrole with axial ligands on the cobalt center (i.e., pyridine and triphenylphosphine) are quite stable.[72] The difference in the electronic structure of corrole macrocycles of **1** and **2** should have an effect on their solution stabilities. To avoid this uncertainty in catalysis, we synthesized the β-brominated analogue **3**, in which these β-pyrrolic substitutions was shown by Dey and Gross to be able to resist oxidative dimerization of metallocoroles.[62] The CV of **3** has two reversible reduction waves at 0.26 V and −1.41 V (Figure 2c). Addition of TFA to an acetonitrile solution of **3** resulted in the rapid growth of the catalytic current (overpotential ∼350 mV, Figure S8). Despite the earlier onset potential, **3** is determined to be less effective as compared to **1** as a HER catalyst mainly because of its limited solubility and smaller catalytic current. Meanwhile, complex **4** having an electron-donating methoxyl substituent is not capable of reducing proton because the active species is generated by reduction at a much more negative potential ($E_{1/2}$ = −2.14 V, Figure 2d). The comparison of the redox chemistry of **1–4** showed that the introduction of electron-withdrawing substituents at the *meso* positions of corrole macrocycles could move the reduction potentials of metal corroles to the anodic direction, which should be favored in lowering the overpotential of electrocatalytic H$_2$ generation. On the basis of these results, the catalytic and mechanistic investigations in the following sections were focused exclusively on **1**.

Catalysis and Stability Evaluation. As shown in Figure 3, the catalytic currents in successive CVs of 0.30 mM **1** in acetonitrile with increasing concentrations of TFA systematically increase until the concentration of TFA reaches 160 mM,
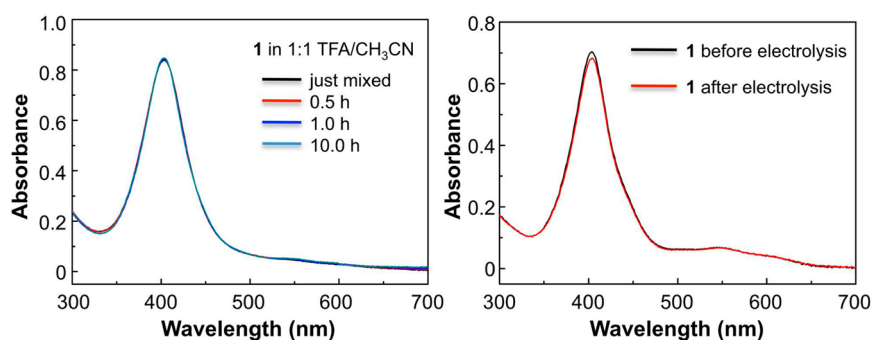
Figure 4. Absorption spectra and stability evaluation of complex **1** in concentrated TFA acid solution (left) and in the electrocatalytic hydrogen evolution (right). Electrolysis conditions: 0.3 mM **1** in acetonitrile with 0.1 M $(NBu_4)PF_6$ supporting electrolyte and 50 μL TFA (160 mM); 2 h electrolysis at −1.50 V.

where the acid-independent region was observed. In our experimental observations, the value of $(i_{cat}/i_p)^2$ increases linearly with acid concentration, indicating a first-order dependence of the catalytic rate on acid concentration (Figure S9). Electrochemical studies revealed that i_{cat} is independent of scan rate ν when the later is larger than 0.5 V s^{-1} (Figure S10), and i_p has a linear correlation with the square root of ν, indicating a diffusion-controlled electrochemical event (Figure S11). It was found that after i_{cat} reached its maximum at the TFA concentration of 160 mM, addition of water could further increase the catalytic current, which might be attributed to the ability of water to enhance proton delivery. Our results showed that by adding 2.24 M water, at an overpotential of 950 mV, a remarkable value of i_{cat}/i_p = 303 could be reached with a scan rate of 100 mV s^{-1} at 20 °C.

The stability of molecular catalysts for H_2 generation in acidic environments is a general concern in designing HER catalysts, although improvement of acid tolerance has been reported in several systems, including synthetic [Fe−Fe] hydrogenase model complexes.[17,26,73−75] Therefore, the stability of **1** in concentrated TFA acetonitrile solution was evaluated (Figure S13). Our results showed that **1** remained unaffected even in a 1:1 (v/v) mixture of TFA and acetonitrile in the dark (Figure 4). The catalyst stability over the course of electrocatalytic H_2 evolution was then verified by UV−vis and NMR spectroscopy before and after electrolysis. As shown in Figure 4 and Figure S14, little to no depletion of UV−visible signal was observed after 2 h of controlled potential electrolysis (CPE) at −1.50 V in the presence of 160 mM TFA, and more than 95% of **1** could be recovered after catalysis as indicated by NMR. Inspection of the glassy carbon working electrode after CPE by SEM and EDX showed no Cu films deposited on the electrode (Figure S15). The corrected electric charges accumulated during electrolysis have a linear dependence on the time (Figure S16), which is a further evidence of the robustness of **1**. The Faradaic efficiency of H_2 production was measured to be >99%, which accounts for 23 turnovers with no detectable decomposition of **1** (Figure S17). All these results support that **1** is stable and has molecular and catalytic nature for generating H_2. It is necessary to note that only catalysts close to the electrode participate in the catalysis, while in reality there are many more catalysts that are not active in the solution. In our calculation, we divided the mole of evolved H_2 by the mole of all catalysts in the solution.

The catalytic HER activity observed for **1** considerably exceeds that reported for the cobalt corrole analogue $[(Cor)Co(py)_2]$ (py = pyridine).[63] Although $[(Cor)Co(py)_2]$

functions well as a heterogeneous electrocatalyst when it was deposited on working electrodes, it degrades by oxidative dimerization after losing its pyridine ligands in acidic solution (see above for discussions), which makes the mechanistic studies challenging. The overpotential required for **1** to generate H_2 is relatively high compared to cobaloxime derivatives.[37,41] However, the i_{cat}/i_p value observed for the latter are typically 1 to 2 orders of magnitude smaller than that for **1**. On the other hand, **1** is as effective as the nickel electrocatalyst recently reported by DuBois,[20] which functions with a i_{cat}/i_p value of 74 at an overpotential of ~1000 mV under similar conditions, and **1** is 1 to 2 orders of magnitude more active than many other nickel bis(diphosphine) complexes operating at comparable overpotentials.[46] More significantly, **1** remains unaffected in concentrated TFA acid solution, while cobaloxime and nickel bis(diphosphine) systems have limited acid tolerance.[20,37,41,46] It is necessary to note that several methods have been proposed in the literature to compare the performance of various molecular HER catalysts.[33,46,76,77] Due to the complexity of the electrocatalytic proton reduction reaction and the difference between diverse systems, direct comparison is challenging. Therefore, in our work, we reported only the i_{cat}/i_p value at certain overpotential, a ratio that has been generally reported in the literature.[33,42,46,78]

Mechanistic Studies. CV studies of **1** with and without TFA (Figure 2 and 3, respectively) showed that the second reversible wave of **1** became a pronounced catalytic wave upon the addition of an external acid. This result indicated that the doubly reduced **1** was likely the catalytic species for proton reduction. To gain more insights into the mechanism of H_2 evolution with **1**, stopped-flow and spectroelectrochemistry experiments were performed. In stopped-flow measurements, **1** was first reduced chemically with sodium borohydride (NaBH$_4$). As shown in Figure 5, reaction of **1** with an excess amount of NaBH$_4$ in acetonitrile resulted in the neat conversion to a new species, which could be tentatively assigned to $[(Cor)Cu]^{2-}$. The characteristic isosbestic point at 413 nm indicated a clean transformation from **1** to its reduced state (Figure S12a). Addition of a large excess of TFA to the resulting solution immediately gave an intermediate with absorption maxima at 328 and 423 nm, which was most probably the hydride intermediate $[(Cor)CuH]^-$. Stopped-flow studies revealed that this hydride intermediate $[(Cor)CuH]^-$ rapidly decayed by reacting with an excess amount of protons to release H_2 and regenerate the initial $[(Cor)Cu]^0$ (Figure S12). It is necessary to note that the reaction mixture was under light irradiation during the entire stopped-flow experiments. As
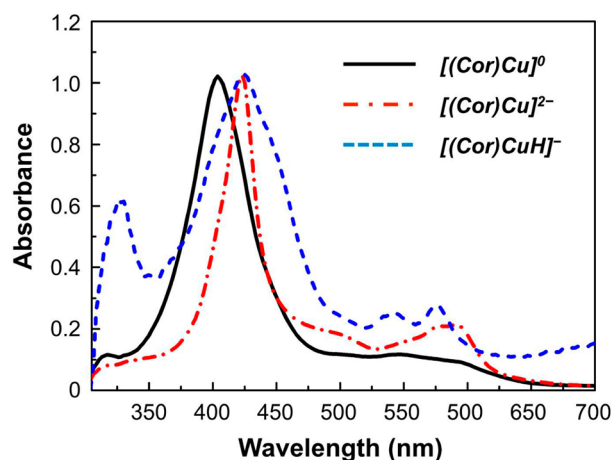
Figure 5. UV−vis spectra of $[(Cor)Cu]^0$, $[(Cor)Cu]^{2-}$ and $[(Cor)$-$CuH]^-$.

Figure 7. Proposed electrocatalytic cycle for H_2 evolution with **1**. There are three possible reaction pathways from hydride intermediate $[(Cor)CuH]^-$ via the reaction with a proton to release H_2 and regenerate the initial $[(Cor)Cu]^0$ (pathway A, black), or via a bimolecular reaction between two such intermediates to form H_2 and $[(Cor)Cu]^-$ (pathway B, green), or via further one-electron reduction to give $[(Cor)CuH]^{2-}$ followed by reaction with a proton to yield H_2 and $[(Cor)Cu]^-$ (pathway C, red).

a result, some levels of degradation of **1** occurred as indicated by the absorption increase around 640 nm.

Controlled potential electrolysis in the absence of TFA in spectroelectrochemistry measurements was performed at −1.50 V, which is more negative than the second reduction peak of **1**. High concentration of **1** was used to enhance the absorption in the range of 500−600 nm, and the solution was protected by ultrapure nitrogen during the entire spectroelectrochemistry measurements. As shown in Figure 6a, the UV−vis spectrum of electrochemically reduced **1** was identical to that observed in stopped-flow measurements by chemical reduction with NaBH$_4$. This result confirmed the formation of $[(Cor)Cu]^{2-}$ in previous stopped-flow experiments. After about a half-hour of electrolysis, most of **1** were converted to its two-electron reduced species. Simulation of the final absorption spectrum showed that more than 80% of **1** were doubly reduced in the controlled potential electrolysis at −1.50 V (see SI and Figure S18). The resemblance in absorption changes between chemical and electrochemical reduction of **1** suggested similar redox behaviors in both chemical and electrochemical systems. Significantly, injection of 1 μL of TFA to the resulting solution caused an immediate growth of the catalytic current and the regeneration of initial $[(Cor)Cu]^0$ (Figure 6b,c). These observations strongly implied that $[(Cor)Cu]^{2-}$ is the catalytic active species to reduce protons.

On the basis of experimental observations, one may envision a catalytic mechanism as illustrated in Figure 7. The reduction
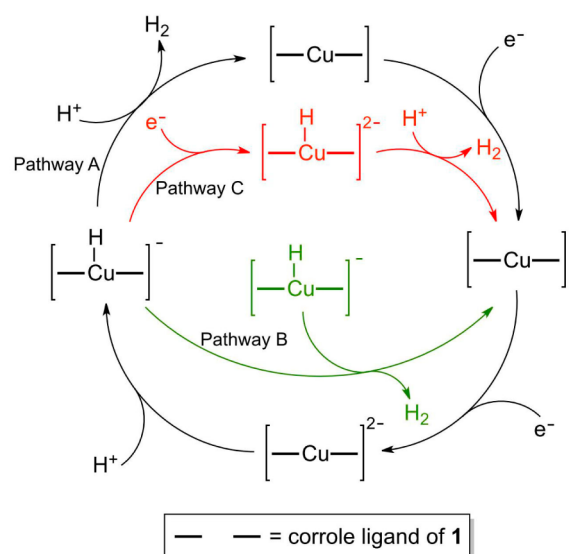
of **1** by two electrons gives the catalytic active species $[(Cor)Cu]^{2-}$ that subsequently reacts with a proton to form a hydride intermediate $[(Cor)CuH]^-$. Then, $[(Cor)CuH]^-$ reacts with a second proton to release H_2 and regenerate the initial $[(Cor)Cu]^0$ (pathway A). The regeneration of $[(Cor)$-$Cu]^0$ in both stopped-flow and spectroelectrochemistry studies indicated that this pathway is feasible under our experimental conditions. However, two other possible reaction pathways for H_2 generation from this hydride intermediate cannot be excluded at this stage. They are (i) a bimolecular reaction between two such intermediates takes place to form H_2 and two equivalents of $[(Cor)Cu]^-$ via the homolysis of the Cu−H bond (pathway B) and (ii) under electrochemical conditions, $[(Cor)CuH]^-$ is further reduced to $[(Cor)CuH]^{2-}$, which then reacts with a proton to yield H_2 and $[(Cor)Cu]^-$ (pathway C).

Theoretical Calculations. Density functional theory (DFT) calculations have been carried out for a better understanding of the H_2 evolution mechanism with **1**. The Cu−corrole complex **1**, which has a closed-shell singlet ground
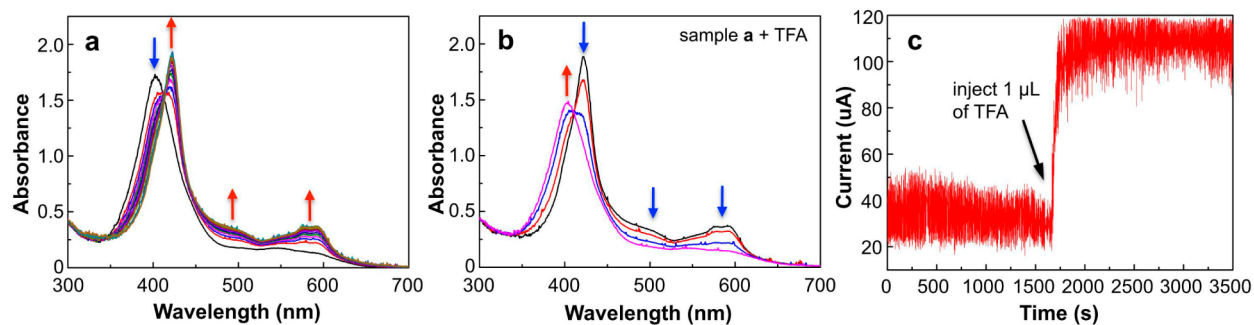

Figure 6. Spectroelectrochemistry experiments. (a) Controlled potential electrolysis of **1** as monitored by UV−vis. (b) The reaction of doubly reduced **1** and TFA monitored by UV−vis. (c) The current curve of **1** during electrolysis at −1.50 V. Electrolysis conditions: 2.2×10^{-5} M **1** in acetonitrile with 0.1 M (NBu$_4$)PF$_6$ electrolyte.

state, can undergo one-electron reduction with a calculated reduction potential of −0.31 V vs ferrocene. The so-generated $[(Cor)Cu]^-$ has a doublet ground state with the single electron occupancy in the σ^*_{xy} orbital (Figure S19), which describes the Cu−N antibonding interactions. This result suggests that the first reduction is largely metal-centered. The second reduction of **1** takes place at the nitrophenyl unit of the corrole ligand as indicated by the singly occupied molecular orbital (Figure S20). The so generated $[(Cor)Cu]^{2-}$ has virtually degenerate open-shell antiferromagnetically coupled singlet and ferromagnetically coupled triplet state with triplet being only 0.69 kcal/mol lower in energy. The calculated potential for the second reduction of **1** is −1.39 V vs ferrocene, which is in a good agreement with the experimental value (−1.42 V vs ferrocene). As shown in Figure 7, the protonation of doubly reduced **1** to form $[(Cor)CuH]^-$ is a general step in the proposed three possible mechanisms for H_2 production (pathway A, B, and C). Our calculated electronic absorption spectrum of the $[(Cor)-CuH]^-$ species agrees well with the experimental spectrum obtained after immediately adding TFA to the doubly reduced **1** (Figure S21), which confirms the formation of such a hydride intermediate. Significantly, the one-electron reduction potential of $[(Cor)CuH]^-$ was calculated to be −1.06 V versus ferrocene, which is 0.33 V more positive than the second reduction potential of **1**. Because pathway A is endergonic and is unlikely to be directly involved in electrocatalysis (see Supporting Information for discussion), it is very likely that in electrochemical experiments, the $[(Cor)CuH]^-$ intermediate can undergo one electron reduction further for subsequent reaction with a proton to form $[(Cor)Cu]^-$ and H_2 (pathway C). However, the combined stopped-flow and absorption spectroscopy experiments indicated that the proton attack on $[(Cor)CuH]^-$ can occur to produce H_2 and regenerate $[(Cor)Cu]^0$ when a high concentration of proton source (TFA) was used.

■ CONCLUSIONS

We have discovered **1** to be an efficient catalyst for H_2 evolution with sufficient stability in concentrated TFA acid solutions. Although proton reduction occurs at moderate overpotentials in acetonitrile, the use of Cu, high i_{cat}/i_p value, and catalyst stability are impressive. As indicated by stopped-flow and spectroelectrochemistry experiments and also DFT calculations, $[(Cor)Cu]^{2-}$ and $[(Cor)CuH]^-$ are key intermediates in catalytic H_2 evolution. Using noninnocent corrole ligands, the redox chemistry of copper is regulated. This result highlights the significant role of redox-active ligands in molecular catalysis[79] and offers considerable contribution to the design of more efficient HER catalysts. Giving the molecular nature of this Cu catalyst, a door may be open for systematic investigation of a large number of related Cu complexes for proton reduction catalysis. Ongoing efforts are focused on detailed mechanistic researches and further improvements of the efficiency and compatibility for light-driven catalytic applications. Examination of copper corroles as catalysts for oxygen evolution is also under investigation as molecular copper complexes have been found, in the last two years,[21,80,81] to be very active for water oxidation.

■ MATERIALS AND METHODS

General Procedures. Manipulations of air- and moisture-sensitive materials were performed under an atmosphere of nitrogen gas using standard Schlenk line techniques. All reagents were purchased from commercial suppliers and used as received unless otherwise noted. Dry solvents, including acetonitrile, dichloromethane, and chloroform, were purified by passage through activated alumina. Corrole ligands, 5,15-pentafluorophenyl-10-(4-nitrophenyl)corrole, 5,10,15-tris-pentafluorophenylcorrole, and 5,15-pentafluorophenyl-10-(4-methoxyphenyl)corrole, were synthesized using modified methods reported previously.[64,66,82−84] ^{1}H NMR spectroscopic measurements were made on a Brüker spectrometer operating at 400 MHz. Electronic absorption spectra were acquired on a Cary 50 spectrophotometer. Infrared spectra (2% sample in KBr) were recorded with a ThermoNicolet Avatar 360 spectrophotometer running the OMNIC software. High-resolution mass spectra were acquired on a Brüker Fourier Transform Ion Cyclotron Resonance Mass Spectrometer APEX IV at Peking University. All stopped-flow data were obtained using a SX20 stopped-flow spectroscopy purchased from the Applied Photophysics Ltd. All UV−vis spectra in stopped-flow studies were recorded in the wavelength range of 300−700 nm at 20 °C.

Synthesis of Complex 1. A solution of 5,15-pentafluorophenyl-10-(4-nitrophenyl)corrole (220 mg, 0.29 mmol) and cupric acetate hydrate (290 mg, 1.46 mmol) in 20 mL of pyridine was stirred at room temperature for 30 min. The solvent was then evaporated, and the purple residue was purified by column chromatography. Fluorescent green-red colored fractions were collected, and recrystallization in chloroform with slow vapor diffusion of *n*-pentane at −10 °C yielded purple crystals of **1** in 2 weeks (154 mg, 0.19 mmol, yield 65%). ^{1}H NMR (400 MHz, CDCl$_3$): δ = 8.38 (d, J = 8.5 Hz, 2H), 8.00 (d, J = 3.5 Hz, 2H), 7.79 (d, J = 8.5 Hz, 2H), 7.46 (d, J = 3.5 Hz, 2H), 7.25 (d, J = 4.5 Hz, 2H); 7.13 (d, J = 4.5 Hz, 2H). FTIR data (2% KBr pellet): 1650 (s), 1596 (s), 1520 (s), 1493 (s), 1442 (sh), 1425 (s), 1343 (s), 1278 (s), 1263 (m), 1174 (m), 1140 (w), 1111 (w), 1064 (s), 1029 (s), 1011 (s), 988 (s), 949 (s), 901 (w), 872 (s), 844 (s), 822 (m), 794 (s), 762 (s), 718 (s), 646 (m), 572 (w), 508 (m). Anal. Calcd for $C_{37}H_{12}CuF_{10}N_5O_2$: C, 54.72; H, 1.49; N, 8.62. Found: C, 55.02; H, 1.60; N, 8.34. High-resolution mass spectrometry: calcd, 811.0127; found, 811.0136 (Figure S1).

Synthesis of Complex 2. A solution of 5,10,15-tris-pentafluorophenylcorrole (147 mg, 0.18 mmol) and cupric acetate hydrate (147 mg, 0.74 mmol) in 15 mL of pyridine was stirred at room temperature for 30 min. The solvent was then evaporated, and the purple residue was purified by column chromatography. Fluorescent green-red colored fractions were collected, and recrystallization in dichloromethane with slow vapor diffusion of *n*-pentane at −10 °C yielded purple crystals of **2** in 2 weeks (100 mg, 0.12 mmol, yield 65%). ^{1}H NMR (400 MHz, CDCl$_3$): δ = 7.97 (d, J = 4.9 Hz, 2H), 7.38 (d, J = 4.9 Hz, 2H), 7.19 (d, J = 4.9 Hz, 2H), 7.02 (d, J = 4.9 Hz, 2H). FTIR data (2% KBr pellet): 1781 (w), 1730 (w), 1650 (s), 1569 (s), 1522 (s), 1493 (s), 1445 (s), 1379 (s), 1329 (s), 1274 (s), 1248 (m), 1176 (s), 1121 (m), 1106 (m), 1081 (s), 1064 (s), 1041 (s), 1022 (s), 992 (s), 953 (s), 935 (s), 889 (s), 847 (s), 822 (m), 796 (m), 763 (s), 752 (s), 738 (s), 702 (m), 683 (m), 643 (w), 530 (w), 504 (w). Anal. Calcd for $C_{37}H_8CuF_{15}N_4$: C, 51.85; H, 0.94; N, 6.54. Found: C, 52.12; H, 1.10; N, 6.34. High-resolution mass spectrometry: calcd, 855.9805; found, 855.9826 (Figure S2).

Synthesis of Complex 3. To a stirred solution of complex **2** (165 mg, 0.19 mmol) in 40 mL of chloroform, was added liquid

bromine (300 μL, 5.7 mmol) dissolved in 16 mL of chloroform over a period of 15 min at room temperature. After the mixture was stirred for 1 h, pyridine (200 μL, 2.5 mmol) dissolved in 16 mL of chloroform was added dropwise over a period of 15 min, and the solution was then stirred for another 1 h. The reaction mixture was shaken with 15 mL of 20% (w/v) aqueous sodium metabisulfite. The organic phase was separated, and the solvent was evaporated. The residue was purified by column chromatography. Fluorescent green colored fractions were collected, and recrystallization in dichloromethane with slow vapor diffusion of n-pentane at -10 °C afforded **3** in 41% yield (114 mg, 0.076 mmol). FTIR data (2% KBr pellet): 1654 (m), 1524 (s), 1500 (s), 1439 (s), 1328 (s), 1272 (s), 1211 (w), 1101 (m), 1083 (m), 1040 (s), 989 (s), 980 (sh), 871 (s), 849 (m), 791 (m), 754 (s), 669 (w). Anal. Calcd for $C_{37}Br_8CuF_{15}N_4$: C, 29.86; N, 3.76. Found: C, 29.55; N, 3.70. High-resolution mass spectrometry: calcd, 1487.2565 (100% peak); found, 1487.2536 (Figure S3).

Synthesis of Complex 4. A solution of 5,15-pentafluorophenyl-10-(4-methoxyphenyl)corrole (300 mg, 0.41 mmol) and cupric acetate hydrate (400 mg, 2.0 mmol) in 30 mL of pyridine was stirred at room temperature for 30 min. The solvent was evaporated, and the purple residue was purified by column chromatography. Fluorescent green-red colored fractions were collected, and recrystallization in dichloromethane with slow vapor diffusion of n-pentane at -10 °C afforded **4** in 71% yield (228 mg, 0.28 mmol). ^{1}H NMR (400 MHz, CDCl$_3$): δ = 7.96 (d, J = 4.0 Hz, 2H), 7.57 (d, J = 8.5 Hz, 2H), 7.46 (d, J = 4.0 Hz, 2H), 7.30 (d, J = 4.4 Hz, 2H), 7.23 (d, J = 4.4 Hz, 2H), 7.03 (d, J = 8.5 Hz, 2H), 3.93 (s, 3H). FTIR data (2% KBr pellet): 1777 (w), 1650 (s), 1603 (s), 1573 (m), 1518 (s), 1493 (s), 1441 (s), 1427 (s), 1402 (m), 1361 (m), 1341 (s), 1299 (s), 1279 (s), 1254 (s), 1178 (s), 1144 (m), 1113 (w), 1064 (s), 1028 (s), 988 (s), 953 (s), 890 (m), 848 (s), 835 (s), 817 (s), 795 (s), 761 (s), 731 (m), 708 (s), 648 (w), 600 (s), 574 (m), 526 (m), 456 (w). Anal. Calcd for $C_{38}H_{15}CuF_{10}N_4O$: C, 57.26; H, 1.90; N, 7.03. Found: C, 57.56; H, 2.01; N, 7.18. High-resolution mass spectrometry: calcd, 796.0382; found, 796.0374 (Figure S4).

Electrochemical Methods. All electrochemical measurements were performed using a CH Instruments (model CHI660E Electrochemical Analyzer). CVs recorded in acetonitrile (0.1 M Bu$_4$NPF$_6$) used a three compartment cell possessing a 0.07 cm^2 glassy carbon electrode as the working electrode, Pt wire as the auxiliary electrode, and Ag as a reference electrode. The solution was bubbled with nitrogen for at least 30 min before analysis, and the purity of the electrolyte medium was confirmed over the available electrochemical window through background scans taken prior to the addition of analyte. Ferrocene was used as an internal standard. The H$_2$ gas produced during electrocatalysis was detected by SP-6890 Gas Chromatograph.

Stability Evaluation of 1 in the Dark. An acetonitrile solution of **1** (4.0×10^{-6} M) with 0.43 M TFA was prepared at room temperature, and its absorption spectrum (300−700 nm) was acquired every 2 h from 0 to 12 h. No detectable decomposition of **1** could be observed after 12 h. In a separate experiment, an acetonitrile solution of **1** (8.0×10^{-6} M) was quickly diluted with an equivolume TFA at room temperature, and the absorption spectrum (300−700 nm) of the resulting solution was recorded immediately after the mixing, and another three spectra were recorded at 0.5, 1.0, and 10 h after the mixing. No detectable decomposition of **1** could be

observed after 10 h in this 1:1 (v/v) mixture of TFA and acetonitrile.

Stability Evaluation of 1 under Irradiation. The sample in the measuring cell was kept under the irradiation of a 150 W Xe-lamp equipped with the SX20 stopped-flow instrument. *In the absence of TFA*: an acetonitrile solution of **1** (7.9×10^{-5} M) was mixed with an equivolume of pure acetonitrile in the measuring cell in the stopped-flow instrument. A UV−vis spectrum (300−700 nm) was recorded immediately after the mixing, and another two spectra were recorded 0.5 and 4.5 h after the mixing. The decomposition of **1** could be observed after 0.5 h, and complete decomposition was observed after 4.5 h. *In the presence of TFA*: an acetonitrile solution of **1** (7.9×10^{-5} M) was mixed with an equivolume of TFA in the measuring cell, and UV−vis spectra (300−700 nm) were recorded. The concentrations of **1** and TFA in the measuring cell were estimated to be 4.0×10^{-5} M and ∼6.5 M. Complex **1** decomposed completely in 2000 s in the presence of a large excess of TFA under Xe-lamp irradiation.

Reduction of 1 by NaBH$_4$ Monitored by Stopped-Flow. A 1.6 mg sample of **1** was dissolved in degassed acetonitrile to a volume of 25.00 mL (7.9×10^{-5} M). NaBH$_4$ (6.0 mg) was dissolved in degassed acetonitrile to a volume of 100.00 mL (1.6×10^{-3} M). The two solutions were mixed in the stopped-flow instrument by a volume ratio of 1:1, and the UV−vis spectra were recorded immediately after the mixing. The concentration of **1** and NaBH$_4$ in the measuring cell of the stopped-flow was estimated to be 4.0×10^{-5} M and 8.0×10^{-4} M, respectively.

Formation and Decay of Hydride Intermediate Monitored by Stopped-Flow. Equivolume acetonitrile solutions of NaBH$_4$ (1.6×10^{-3} M) and **1** (7.9×10^{-5} M) were mixed in the premix cell equipped with the SX20 stopped-flow instrument for 1 min for quantitative conversion of **1** to $[(Cor)Cu]^{2-}$. A freshly prepared acetonitrile solution of TFA (0.316 M) and the premixed solution were then injected and mixed in the cell with a volume ratio of 1:1. The formation of the hydride intermediate $[(Cor)CuH]^-$ was monitored by absorption spectroscopy immediately after the mixing. The concentrations of **1**, NaBH$_4$, and TFA in the measuring cell in the stopped-flow instrument were estimated to be 2.0×10^{-5}, 4.0×10^{-4} and 0.158 M, respectively. The absorption of this hydride intermediate reached the maximum in 2 s and started to decay after that. It is worth noting that less than 2.40×10^{-2} μmol of H$_2$ would be formed in this process in a 20 μL optical cell equipped with the stopped-flow instrument. As it is known that 6.85×10^{-2} μmol of H$_2$ could be dissolved in 20 μL of acetonitrile,[85] the generated H$_2$ will have negligible influence on the measurement.

Controlled Potential UV−vis Spectroelectrochemistry Studies of 1. A three-electrode configuration was employed using a CH Instruments potentiostat with CH Instruments 840B software. The glassy-carbon working electrode (1 mm diameter) was treated in a sequence of polishing by alumina oxide (0.25 μm) and washing by ethanol and deionized water. Ag and Pt wires were used as the reference and counter electrodes, respectively. A 4.8 mg sample of **1** was dissolved in 25.00 mL of degassed acetonitrile with 0.1 M (NBu$_4$)PF$_6$ as the electrolyte, and 300 μL of this resulting solution was further diluted by another 3.0 mL of 0.1 M (NBu$_4$)PF$_6$ acetonitrile solution to make the final concentration of **1** to be 2.2×10^{-5} M, which is capable for UV−vis measurements. The solution was added into a quartz cell equipped with an electrochemical

setup and was bubbled by ultrapure nitrogen (presaturated with acetonitrile vapor) during UV−vis spectroelectrochemistry measurements at controlled potential electrolysis −1.50 V. UV−vis spectra (300−700 nm) were recorded using the SHIMADZU UV-3100 UV−vis-NIR spectrophotometer during the electrolysis. After electrolysis, 1 μL of TFA was injected into the quartz cell using microsyringe, and UV−vis spectra were then recorded.

Computational Details. All calculations were performed using the density functional theory (DFT) functional BP86/def-SVP as implemented in the Gaussian 09 software.[86] Solvent effect was considered in all geometry optimizations and property calculations using the conductor-like polarizable continuum model (CPCM).[87] The absorption spectrum of the hydride intermediate was calculated using the time-dependent DFT method at the same level. The energies were corrected by single point calculations using a larger basis set, Def2-TZVP for all the atoms. For the absolute solvation free energy of the proton in acetonitrile, a value of −260.2 kcal/mol was used.[88] Reference potential of NHE was set at −4.28 V for the redox potential calculations. The potentials relative to ferrocene were then calculated by assuming ferrocene to be 0.40 V vs NHE in water.

■ ASSOCIATED CONTENT

ⓢ Supporting Information

The Supporting Information is available free of charge on the ACS Publications website at DOI: 10.1021/acscatal.5b00666.

> Absorption spectrum simulation studies; X-ray diffraction studies; Figures S1−S21; Table S1; Cartesian coordinates for the key species (PDF)
> Crystallographic data as CIFs for complex **1** (CCDC 988459)(CIF)
> Crystallographic data as CIFs for complex **2** (CCDC 988460)(CIF)

■ AUTHOR INFORMATION

Corresponding Authors

*E-mail: ruicao@ruc.edu.cn.
*E-mail: fuxf@pku.edu.cn.
*E-mail: wenzhenlai@ruc.edu.cn.

Author Contributions

∥H.L. and H.F. contributed equally to this work.

Notes

The authors declare no competing financial interest.

■ ACKNOWLEDGMENTS

■ REFERENCES

(1) Grätzel, M. *Nature* **2001**, *414*, 338−344.

(2) Gray, H. B. *Nat. Chem.* **2009**, *1*, 7−7.

(3) Cao, R.; Lai, W. Z.; Du, P. W. *Energy Environ. Sci.* **2012**, *5*, 8134−8157.

(4) Cook, T. R.; Dogutan, D. K.; Reece, S. Y.; Surendranath, Y.; Teets, T. S.; Nocera, D. G. *Chem. Rev.* **2010**, *110*, 6474−6502.

(5) Nocera, D. G. *Acc. Chem. Res.* **2012**, *45*, 767−776.

(6) McKone, J. R.; Lewis, N. S.; Gray, H. B. *Chem. Mater.* **2014**, *26*, 407−414.

(7) Wu, Y. Z.; Chen, M. X.; Han, Y. Z.; Luo, H. X.; Su, X. J.; Zhang, M.-T.; Lin, X. H.; Sun, J. L.; Wang, L.; Deng, L.; Zhang, W.; Cao, R. *Angew. Chem., Int. Ed.* **2015**, *54*, 4870−4875.

(8) Dempsey, J. L.; Brunschwig, B. S.; Winkler, J. R.; Gray, H. B. *Acc. Chem. Res.* **2009**, *42*, 1995−2004.

(9) Le Goff, A.; Artero, V.; Jousselme, B.; Tran, P. D.; Guillet, N.; Métayé, R.; Fihri, A.; Palacin, S.; Fontecave, M. *Science* **2009**, *326*, 1384−1387.

(10) Wang, F.; Wang, W. G.; Wang, H. Y.; Si, G.; Tung, C. H.; Wu, L. Z. *ACS Catal.* **2012**, *2*, 407−416.

(11) Han, Z. J.; Qiu, F.; Eisenberg, R.; Holland, P. L.; Krauss, T. D. *Science* **2012**, *338*, 1321−1324.

(12) Jacques, P. A.; Artero, V.; Pécaut, J.; Fontecave, M. *Proc. Natl. Acad. Sci. U. S. A.* **2009**, *106*, 20627−20632.

(13) Andreiadis, E. S.; Jacques, P. A.; Tran, P. D.; Leyris, A.; Chavarot-Kerlidou, M.; Jousselme, B.; Matheron, M.; Pécaut, J.; Palacin, S.; Fontecave, M.; Artero, V. *Nat. Chem.* **2013**, *5*, 48−53.

(14) Hu, P.; Diskin-Posner, Y.; Ben-David, Y.; Milstein, D. *ACS Catal.* **2014**, *4*, 2649−2652.

(15) Onoda, A.; Kihara, Y.; Fukumoto, K.; Sano, Y.; Hayashi, T. *ACS Catal.* **2014**, *4*, 2645−2648.

(16) Morales-Guio, C. G.; Tilley, S. D.; Vrubel, H.; Grätzel, M.; Hu, X. L. *Nat. Commun.* **2014**, *5*, 3059.

(17) Dey, S.; Rana, A.; Dey, S. G.; Dey, A. *ACS Catal.* **2013**, *3*, 429−436.

(18) Solis, B. H.; Maher, A. G.; Honda, T.; Powers, D. C.; Nocera, D. G.; Hammes-Schiffer, S. *ACS Catal.* **2014**, *4*, 4516−4526.

(19) Chen, L. J.; Chen, G.; Leung, C. F.; Yiu, S. M.; Ko, C. C.; Anxolabéhère-Mallart, E.; Robert, M.; Lau, T. C. *ACS Catal.* **2015**, *5*, 356−364.

(20) Helm, M. L.; Stewart, M. P.; Bullock, R. M.; DuBois, M. R.; DuBois, D. L. *Science* **2011**, *333*, 863−866.

(21) Barnett, S. M.; Goldberg, K. I.; Mayer, J. M. *Nat. Chem.* **2012**, *4*, 498−502.

(22) Lubitz, W.; Ogata, H.; Rüdiger, O.; Reijerse, E. *Chem. Rev.* **2014**, *114*, 4081−4148.

(23) Fontecilla-Camps, J. C.; Volbeda, A.; Cavazza, C.; Nicolet, Y. *Chem. Rev.* **2007**, *107*, 4273−4303.

(24) Tard, C.; Pickett, C. J. *Chem. Rev.* **2009**, *109*, 2245−2274.

(25) Plumeré, N.; Rüdiger, O.; Oughli, A. A.; Williams, R.; Vivekananthan, J.; Pöller, S.; Schuhmann, W.; Lubitz, W. *Nat. Chem.* **2014**, *6*, 822−827.

(26) Dey, S.; Rana, A.; Crouthers, D.; Mondal, B.; Das, P. K.; Darensbourg, M. Y.; Dey, A. *J. Am. Chem. Soc.* **2014**, *136*, 8847−8850.

(27) Artero, V.; Chavarot-Kerlidou, M.; Fontecave, M. *Angew. Chem., Int. Ed.* **2011**, *50*, 7238−7266.

(28) Wang, M.; Chen, L.; Sun, L. C. *Energy Environ. Sci.* **2012**, *5*, 6763−6778.

(29) McKone, J. R.; Marinescu, S. C.; Brunschwig, B. S.; Winkler, J. R.; Gray, H. B. *Chem. Sci.* **2014**, *5*, 865−878.

(30) Ran, J. R.; Zhang, J.; Yu, J. G.; Jaroniec, M.; Qiao, S. Z. *Chem. Soc. Rev.* **2014**, *43*, 7787−7812.

(31) Faber, M. S.; Jin, S. *Energy Environ. Sci.* **2014**, *7*, 3519−3542.

(32) Tard, C.; Liu, X. M.; Ibrahim, S. K.; Bruschi, M.; De Gioia, L.; Davies, S. C.; Yang, X.; Wang, L. S.; Sawers, G.; Pickett, C. J. *Nature* **2005**, *433*, 610−613.

(33) Rose, M. J.; Gray, H. B.; Winkler, J. R. *J. Am. Chem. Soc.* **2012**, *134*, 8310−8313.

(34) Berggren, G.; Adamska, A.; Lambertz, C.; Simmons, T. R.; Esselborn, J.; Atta, M.; Gambarelli, S.; Mouesca, J. M.; Reijerse, E.; Lubitz, W.; Happe, T.; Artero, V.; Fontecave, M. *Nature* **2013**, *499*, 66−69.

(35) Li, X. Q.; Wang, M.; Zheng, D. H.; Han, K.; Dong, J. F.; Sun, L. C. *Energy Environ. Sci.* **2012**, *5*, 8220−8224.

(36) Hu, X. L.; Cossairt, B. M.; Brunschwig, B. S.; Lewis, N. S.; Peters, J. C. *Chem. Commun.* **2005**, 4723−4725.

(37) Hu, X. L.; Brunschwig, B. S.; Peters, J. C. *J. Am. Chem. Soc.* **2007**, *129*, 8988−8998.

(38) Lee, C. H.; Dogutan, D. K.; Nocera, D. G. *J. Am. Chem. Soc.* **2011**, *133*, 8775−8777.

(39) Sun, Y. J.; Bigi, J. P.; Piro, N. A.; Tang, M. L.; Long, J. R.; Chang, C. J. *J. Am. Chem. Soc.* **2011**, *133*, 9212−9215.

(40) Stubbert, B. D.; Peters, J. C.; Gray, H. B. *J. Am. Chem. Soc.* **2011**, *133*, 18070−18073.

(41) Valdez, C. N.; Dempsey, J. L.; Brunschwig, B. S.; Winkler, J. R.; Gray, H. B. *Proc. Natl. Acad. Sci. U. S. A.* **2012**, *109*, 15589−15593.

(42) Marinescu, S. C.; Winkler, J. R.; Gray, H. B. *Proc. Natl. Acad. Sci. U. S. A.* **2012**, *109*, 15127−15131.

(43) Kleingardner, J. G.; Kandemir, B.; Bren, K. L. *J. Am. Chem. Soc.* **2014**, *136*, 4−7.

(44) Chen, L.; Wang, M.; Han, K.; Zhang, P. L.; Gloaguen, F.; Sun, L. C. *Energy Environ. Sci.* **2014**, *7*, 329−334.

(45) Zhang, P. L.; Wang, M.; Gloaguen, F.; Chen, L.; Quentel, F.; Sun, L. C. *Chem. Commun.* **2013**, *49*, 9455−9457.

(46) Kilgore, U. J.; Roberts, J. A. S.; Pool, D. H.; Appel, A. M.; Stewart, M. P.; DuBois, M. R.; Dougherty, W. G.; Kassel, W. S.; Bullock, R. M.; DuBois, D. L. *J. Am. Chem. Soc.* **2011**, *133*, 5861−5872.

(47) Karunadasa, H. I.; Chang, C. J.; Long, J. R. *Nature* **2010**, *464*, 1329−1333.

(48) Karunadasa, H. I.; Montalvo, E.; Sun, Y. J.; Majda, M.; Long, J. R.; Chang, C. J. *Science* **2012**, *335*, 698−702.

(49) Thoi, V. S.; Karunadasa, H. I.; Surendranath, Y.; Long, J. R.; Chang, C. J. *Energy Environ. Sci.* **2012**, *5*, 7762−7770.

(50) Mirica, L. M.; Ottenwaelder, X.; Stack, T. D. P. *Chem. Rev.* **2004**, *104*, 1013−1045.

(51) Lewis, E. A.; Tolman, W. B. *Chem. Rev.* **2004**, *104*, 1047−1076.

(52) Yu, J. G.; Ran, J. R. *Energy Environ. Sci.* **2011**, *4*, 1364−1371.

(53) Maeda, K.; Ohno, T.; Domen, K. *Chem. Sci.* **2011**, *2*, 1362−1368.

(54) Paracchino, A.; Mathews, N.; Hisatomi, T.; Stefik, M.; Tilley, S. D.; Grätzel, M. *Energy Environ. Sci.* **2012**, *5*, 8673−8681.

(55) Tran, P. D.; Nguyen, M.; Pramana, S. S.; Bhattacharjee, A.; Chiam, S. Y.; Fize, J.; Field, M. J.; Artero, V.; Wong, L. H.; Loo, J.; Barber, J. *Energy Environ. Sci.* **2012**, *5*, 8912−8916.

(56) Schouten, K. J. P.; Qin, Z. S.; Gallent, E. P.; Koper, M. T. M. *J. Am. Chem. Soc.* **2012**, *134*, 9864−9867.

(57) Li, C. W.; Kanan, M. W. *J. Am. Chem. Soc.* **2012**, *134*, 7231−7234.

(58) Li, C. W.; Ciston, J.; Kanan, M. W. *Nature* **2014**, *508*, 504−507.

(59) Chen, Z. F.; Ye, S. R.; Wilson, A. R.; Ha, Y. C.; Wiley, B. J. *Energy Environ. Sci.* **2014**, *7*, 1461−1467.

(60) Zhang, P. L.; Wang, M.; Yang, Y.; Yao, T. Y.; Sun, L. C. *Angew. Chem., Int. Ed.* **2014**, *53*, 13803−13807.

(61) Mondal, B.; Sengupta, K.; Rana, A.; Mahammed, A.; Botoshansky, M.; Dey, S. G.; Gross, Z.; Dey, A. *Inorg. Chem.* **2013**, *52*, 3381−3387.

(62) Mahammed, A.; Mondal, B.; Rana, A.; Dey, A.; Gross, Z. *Chem. Commun.* **2014**, *50*, 2725−2727.

(63) Lei, H. T.; Han, A. L.; Li, F. W.; Zhang, M. N.; Han, Y. Z.; Du, P. W.; Lai, W. Z.; Cao, R. *Phys. Chem. Chem. Phys.* **2014**, *16*, 1883−1893.

(64) Wasbotten, I. H.; Wondimagegn, T.; Ghosh, A. *J. Am. Chem. Soc.* **2002**, *124*, 8104−8116.

(65) Thomas, K. E.; Alemayehu, A. B.; Conradie, J.; Beavers, C. M.; Ghosh, A. *Acc. Chem. Res.* **2012**, *45*, 1203−1214.

(66) Luobeznova, I.; Simkhovich, L.; Goldberg, I.; Gross, Z. *Eur. J. Inorg. Chem.* **2004**, *2004*, 1724−1732.

(67) Dogutan, D. K.; McGuire, R., Jr.; Nocera, D. G. *J. Am. Chem. Soc.* **2011**, *133*, 9178−9180.

(68) Fang, H.; Ling, Z.; Brothers, P. J.; Fu, X. *Chem. Commun.* **2011**, *47*, 11677−11679.

(69) Lai, W. Z.; Cao, R.; Dong, G.; Shaik, S.; Yao, J. N.; Chen, H. *J. Phys. Chem. Lett.* **2012**, *3*, 2315−2319.

(70) Fang, H.; Ling, Z.; Lang, K.; Brothers, P. J.; de Bruin, B.; Fu, X. *Chem. Sci.* **2014**, *5*, 916−921.

(71) Felton, G. A. N.; Glass, R. S.; Lichtenberger, D. L.; Evans, D. H. *Inorg. Chem.* **2006**, *45*, 9181−9184.

(72) Mahammed, A.; Giladi, I.; Goldberg, I.; Gross, Z. *Chem. - Eur. J.* **2001**, *7*, 4259−4265.

(73) Felton, G. A. N.; Vannucci, A. K.; Chen, J. Z.; Lockett, L. T.; Okumura, N.; Petro, B. J.; Zakai, U. I; Evans, D. H.; Glass, R. S.; Lichtenberger, D. L. *J. Am. Chem. Soc.* **2007**, *129*, 12521−12530.

(74) Liang, W. J.; Wang, F.; Wen, M.; Jian, J. X.; Wang, X. Z.; Chen, B.; Tung, C. H.; Wu, L. Z. *Chem. - Eur. J.* **2015**, *21*, 3187−3192.

(75) Quentel, F.; Passard, G.; Gloaguen, F. *Energy Environ. Sci.* **2012**, *5*, 7757−7761.

(76) Costentin, C.; Drouet, S.; Robert, M.; Savéant, J. M. *J. Am. Chem. Soc.* **2012**, *134*, 11235−11242.

(77) Costentin, C.; Passard, G.; Savéant, J. M. *J. Am. Chem. Soc.* **2015**, *137*, 5461−5467.

(78) Stewart, M. P.; Ho, M. H.; Wiese, S.; Lindstrom, M. L.; Thogerson, C. E.; Raugei, S.; Bullock, R. M.; Helm, M. L. *J. Am. Chem. Soc.* **2013**, *135*, 6033−6046.

(79) Luca, O. R.; Crabtree, R. H. *Chem. Soc. Rev.* **2013**, *42*, 1440−1459.

(80) Zhang, M.-T.; Chen, Z. F.; Kang, P.; Meyer, T. J. *J. Am. Chem. Soc.* **2013**, *135*, 2048−2051.

(81) Zhang, T.; Wang, C.; Liu, S. B.; Wang, J. L.; Lin, W. B. *J. Am. Chem. Soc.* **2014**, *136*, 273−281.

(82) Xia, M.; Liu, J. H.; Gao, Y.; Åkermark, B.; Sun, L. C. *Helv. Chim. Acta* **2007**, *90*, 553−561.

(83) Gao, Y.; Liu, J. H.; Jiang, W. F.; Xia, M.; Zhang, W.; Li, M. N.; Åkermark, B.; Sun, L. C. *J. Porphyrins Phthalocyanines* **2007**, *11*, 463−469.

(84) Alemayehu, A.; Conradie, M. M.; Ghosh, A. *J. Porphyrins Phthalocyanines* **2012**, *16*, 695−704.

(85) Brunner, E. *J. Chem. Eng. Data* **1985**, *30*, 269−273.

(86) Frisch, M. J.; Trucks, G. W.; Schlegel, H. B.; Scuseria, G. E.; Robb, M. A.; Cheeseman, J. R.; Scalmani, G.; Barone, V.; Mennucci, B.; Petersson, G. A.; Nakatsuji, H.; Caricato, M.; Li, X.; Hratchian, H. P.; Izmaylov, A. F.; Bloino, J.; Zheng, G.; Sonnenberg, J. L.; Hada, M.; Ehara, M.; Toyota, K.; Fukuda, R.; Hasegawa, J.; Ishida, M.; Nakajima, T.; Honda, Y.; Kitao, O.; Nakai, H.; Vreven, T.; Montgomery, J. A. J.; Peralta, J. E.; Ogliaro, F.; Bearpark, M.; Heyd, J. J.; Brothers, E.; Kudin, K. N.; Staroverov, V. N.; Keith, T.; Kobayashi, R.; Normand, J.; Raghavachari, K.; Rendell, A.; Burant, J. C.; Iyengar, S. S.; Tomasi, J.; Cossi, M.; Rega, N.; Millam, N. J.; Klene, M.; Knox, J. E.; Cross, J. B.; Bakken, V.; Adamo, C.; Jaramillo, J.; Gomperts, R.; Stratmann, R. E.; Yazyev, O.; Austin, A. J.; Cammi, R.; Pomelli, C.; Ochterski, J. W.; Martin, R. L.; Morokuma, K.; Zakrzewski, V. G.; Voth, G. A.; Salvador, P.; Dannenberg, J. J.; Dapprich, S.; Daniels, A. D.; Farkas, Ö.; Foresman, J. B.; Ortiz, J. V.; Cioslowski, J.; Fox, D. J. *Gaussian 09*, Revision C.01; Gaussian, Inc.: Wallingford, CT, 2010.

(87) Barone, V.; Cossi, M. *J. Phys. Chem. A* **1998**, *102*, 1995−2001.

(88) Kelly, C. P.; Cramer, C. J.; Truhlar, D. G. *J. Phys. Chem. B* **2007**, *111*, 408−422.